Comparison of flow modification induced by plasma and fluidic jet actuators dedicated to circulation control around wind turbine airfoils

A. Leroy, Caroline Braud, S. Baleriola, S. Loyer, Philippe Devinant, S. Aubrun

Comparison of flow modification induced by plasma and fluidic jet actuators dedicated to circulation control around wind turbine airfoils

2016 J. Phys.: Conf. Ser. 753 022012

(http://iopscience.iop.org/1742-6596/753/2/022012)

Comparison of flow modification induced by plasma and fluidic jet actuators dedicated to circulation control around wind turbine airfoils

A. Leroy*, C. Braud, S. Baleriola*, S. Loyer*, P. Devinant*, S. Aubrun***

*Université d'Orléans, INSA CVL, PRISME, EA 4229, F-45072, Orléans, France
**LHEEA, Ecole Centrale Nantes, F-44321 Nantes Cedex 3, France

Corresponding author's e-mail address : annie.leroy@univ-orleans.fr

Abstract. In order to reduce the aerodynamic load fluctuations on wind turbine blades by innovative control solutions, strategies of active circulation control acting at the blade airfoil trailing edge are studied, allowing lift increase and decrease. This study presents a comparison of results obtained by performing surface plasma and continuous fluidic jet actuation on a blade airfoil designed with a rounded trailing edge. In the present study, both actuator types are located at the trailing edge. Plasma actuators act uniformly in the spanwise direction, whereas fluidic jets blow through small squared holes distributed along the span, and therefore, provide a three-dimensional action on the flow. Load and velocity field measurements were performed to assess the effectiveness of both actuators and to highlight the flow mechanisms induced by both actuation methods for lift-up configurations. Results are presented for a chord Reynolds number of 2. 10^5 and for a lift coefficient increase of 0.06.

1. Introduction

Circulation control strategies for aerodynamic bodies are traditionally implemented by means of concepts including shape change, flaps, blowing, suction, etc., and often make use of the Coanda effect that keeps a tangential jet attached over a curved surface. Initially, applications focused on fixed wind aircraft and were progressively applied to any control surface (flap, aileron, engine, propeller...), then submarine-hydrodynamics and rotary wings. The main objective was to increase the circulation around the aerodynamic body, and so the lift force, by acting at the trailing edge when large lifting forces and/or slow speeds were required, such as at take-off and landing of aircraft. One can find a survey of circulation control applications in [1, 2]. Recent applications are turned nowadays towards wind turbines [3-4] and water turbines. Incoming wind conditions for wind turbines are strongly inhomogeneous and unsteady. In order to reduce the aerodynamic load fluctuations on wind turbine blades considering a given operating case, innovative control concepts based on such strategies are investigated because high expectations exist. Due to inhomogeneous and unsteady incoming flow, it is expected that wind turbine airfoils under real operating conditions may encounter variation of $\pm 5°$ around in angles of attack inducing load variations to mitigate. It is then necessary to optimize the wind energy efficiency by developing innovative control concepts with the intention of reducing load fluctuations on blades. The cost of energy will be therefore reduced by extending the lifetime of the wind turbine rotors. As a first stage, the objective of this study is to assess the potentialities of circulation control techniques. The

baseline aerodynamic configuration is a fully attached flow on the airfoil, and the final objective of the control is to maintain the lift at a fixed value, whatever the incoming flow disturbances.

Circulation control strategy can be achieved by using blowing along a rounded airfoil trailing edge in order to manipulate the separation point of the boundary layer at the trailing edge, leading to the modification of the circulation around the aerodynamic airfoil, and so, the lift, as illustrated in figure 1. Indeed, the jet evolving along the round surface is an effective boundary layer control, it allows to delay boundary layer separation and can lead to a delayed stagnation point position. In order to fully take advantages of the Coanda effect along curved surface in view of high lift increase (super-circulation), it is usually necessary for conventional blowing to be characterized by a high momentum coefficient as exposed in [1].

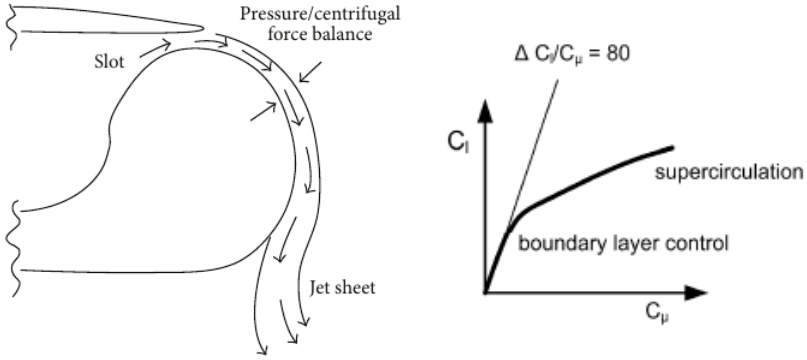

Figure 1. Principle of circulation control based on blowing and Coanda effects and lift coefficient versus momentum coefficient from [1].

In this study, two methods of active flow control acting at the blade airfoil trailing edge are investigated allowing lift increase and compared in terms of load efficiency and induced flow mechanisms. Two types of actuators are used in this circulation control application: dielectric barrier discharges (DBD) as surface plasma actuators and fluidic jet distribution. Both actuators are characterised by quite low momentum coefficients and allow to perform a bi-dimensional and a three-dimensional action on the flow respectively. It is assumed that the flow induced by the DBD actuator behaves like a two-dimensional wall jet whereas jets don't act uniformly in the spanwise direction since they are discretely distributed and therefore, provide a three-dimensional action.

Interest in plasma actuators for flow control has been largely reported in the literature over the last decade. Recent papers [5-6] give an overview of various configurations based on the surface Dielectric Barrier Discharge (DBD). The potentialities of this type of actuator to manipulate flows have been largely studied for boundary layer control and transition control as reviewed in [7]. Recent studies have dealt with control circulation by surface plasma actuators [8-9] in which the feasibility of this strategy was demonstrated. The second control method concerns the use of continuous fluidic jet distribution, more conventionally used for turbulent boundary layer separation control. Indeed, when fluidic round jets are inclined relatively to the wall and to the main stream of the baseline flow, they are able to generate streamwise vortices qualitatively similar to those of passive vortex generators [10-11]. By comparing slot jet control and discrete round jets control, experimentally and numerically on the same configuration [12-13], it was found that the most efficient control is obtained when the structures resulting from the interaction of the control jet with the cross-flow (streamwise or spanwise), have a long enough coherence to reinforce the turbulent boundary subjected to an adverse pressure gradient.

This paper focuses on a comparison of results obtained by performing plasma and continuous jet actuation on a blade airfoil designed with a rounded trailing edge. Time averaged aerodynamic values and flow field measurements were performed to assess the effectiveness of both actuator types located at the trailing edge and to focus on flow mechanisms involved in this type of flow control strategy for a given operating lift coefficient increment.

2. Experimental set-up

2.1. Circulation control oriented airfoil model

In order to enable a circulation control through continuous jets (CJ) or plasma actuators (PA) of an attached flow around an airfoil, it is necessary to make the trailing edge round. For this study, the trailing edge of the generic NACA65$_4$- 421 profile was replaced by a rounded one with a radius of curvature of 2% of the chord. The shape adjustment between the modified trailing edge and the pressure side was designed in order to increase the airfoil camber, as a compensation for the expected degradation of the drag due to the thickening of the trailing edge. Figure 2 shows the comparison between the generic NACA65$_4$- 421 airfoil profile and the CC-oriented airfoil profile NACA65$_4$- 421--CC. The NACA65$_4$-421-CC airfoil model used for this study has a chord of c = 300 mm and a wing span of 1.1 m.

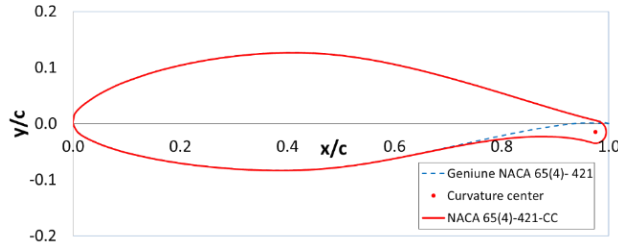

Figure 2. Section view of the control circulation oriented NACA65$_4$-421-CC.

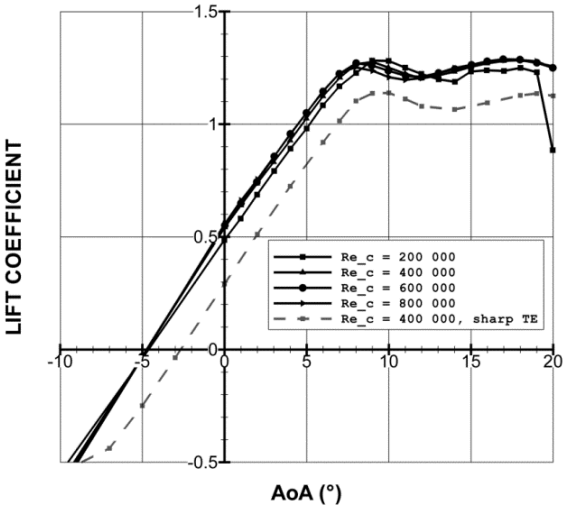

Figure 3. Lift coefficient versus angle of attack (AOA) for different Reynolds numbers.

2.2. The wind tunnel and experimental equipment

The experiments were carried out at the PRISME laboratory of University of Orleans, in its closed return wind tunnel. Two airfoils having the NACA65$_4$-421-CC profile have been specifically designed respectively for PA or CJ purposes as described in the next section. The airfoil was then mounted horizontally between two vertical flat planes in order to achieve a 2D flow configuration into the 5 m long main test section with a cross-section of 2 m × 2 m. It was mounted on both tips onto a 6-component ground balance used for time-averaged lift and drag measurements and located under the test section. The balance was carefully calibrated, lift and drag coefficient uncertainties were estimated at 10 m/s to be less than 5 % for the lift force and 10 % for the drag force. In the present study, the operating speed of the wind tunnel varied from 7 m/s to 40 m/s with an airflow turbulence level below 0.4 %. For the NACA65$_4$-421-CC airfoil, figure 3 shows the lift coefficients C_L measured with the aerodynamic balance versus the airfoil angle of attack α for different Reynolds numbers based on the chord length. It shows that C_L does not depend on the Reynolds number for higher Reynolds numbers (from 4. 10^5) since the curves are superimposed. For the lower Reynolds number, the curve is slightly different all over the AOA range but dramatically changes for higher AOA (more than 18 °), when the stall appears earlier than for higher Reynolds number configurations. The maximum C_L = 1.27 is obtained at an AOA of 8-9 °. From 9° to 20 ° AOAs, C_L saturates due to the separation area on the suction side of the airfoil. In this study, results will be presented for a Reynolds number of 2. 10^5 and for an AOA of 5 ° corresponding to an attached flow along the suction side.

Mean pressure distribution around the airfoil was measured with pressure taps implemented around the model. 20 pressure taps are available for the PA airfoil in the median section. For the CJ airfoil, 42 pressure taps are distributed chordwise at different positions along the span of the airfoil because it is made of a stack of 2D profiles. The stack of these 2D profiles provides a plenum chamber in the transverse direction that can be connected indifferently by a compressed air system or by a pressure manometer. The orifices located at the same chord position are then connected in the transverse direction and to the pressure manometer. Consequently, for the CJ airfoil, pressure measurement values are then the result of a space-average in the transverse direction. Mean velocity fields around the airfoil trailing edge were studied from 2D-PIV measurements in order to analyze flow topology in longitudinal planes of the airfoil model and more particularly in the median plane (z = 0 mm). The PIV system consisted, in the case of the wind-tunnel experiments, in a Nd:Yag laser (2 × 200 mJ) emitting pulses with a 2.5 Hz emission rate. The light sheet was oriented in order to visualize simultaneously both pressure and suction sides of the airfoil. Seeding particles were micro-sized olive oil droplets sprayed by a PIVTEC seeding system. Images were acquired with a LaVision Imager LX camera (4032 px × 2688 px) and a 200 mm lens. 1,000 image pairs were recorded. For CJ configuration, vector fields were computed using OpenPIV Software running in parallel [14]. A signal to noise ratio of 1.3 and a threshold filter on velocity components were used to validate the vector field. The final resolution is of one vector every 0.8 mm with a 32 px × 32 px interrogation window. For PA configuration, images processing was carried out with DaVis 8.3 LaVision software and the final resolution is of one vector every 0.4 mm with a 32 px × 32 px interrogation window with an overlap of 50%. For the quiescent air experiments, the same seeding system was used as well as a similar laser. The camera used was a TSI Power View (2048 px × 2048 px) with a 200 mm lens. 600 image pairs were recorded for every configuration. This system allows a final resolution of one vector every 0.5 mm with a 32 px × 32 px interrogation window.

2.3. DBD actuator

Figure 4 shows the section view of the trailing edge airfoil sections equipped with the DBD actuator made of two successive single DBD. One single DBD consists in two copper electrodes that are positioned on both sides of a dielectric material (PMMA, 3 mm thick). The high voltage electrodes (or active electrodes) are serrated and powered with an AC-power supply up to 18 kV and 1 kHz, while the grounded one is linear and encapsulated within the dielectric material of the model itself. The high voltage and grounded electrodes were 950 mm long, while the length of the floating electrode was 900 mm. With a high voltage application at the active electrode, the ambient air is ionized and accelerated, creating an ionic wind along the grounded electrode that permits the manipulation of the flow near the wall zone. For such an actuator, the electrical power consumption was measured and estimated at around 40 W/m. By considering same electrical parameters, the power consumption usually remains about the same without and with incoming flow. It is assumed that the flow induced by this actuator behaves like a two-dimensional wall jet. It was characterized in quiescent air conditions by PIV in the median airfoil section. As shown in figure 5, the ambient air is deflected towards the plasma region with a strong acceleration close to the wall, highlighting the higher velocity at the plasma-gas interface along the whole actuator. Downstream of the main actuation zone, one can observe diffusion of the induced jet on the normal direction to the wall. The velocity vector profiles suggest that the wall jet expands away from the wall because of the curvature resulting in a widened jet in the pressure side zone with slight lower longitudinal velocities.

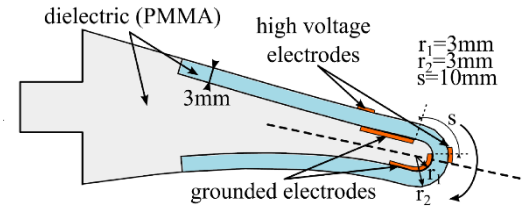

Figure 4. Scheme of the trailing edge equipped with the DBD actuator.

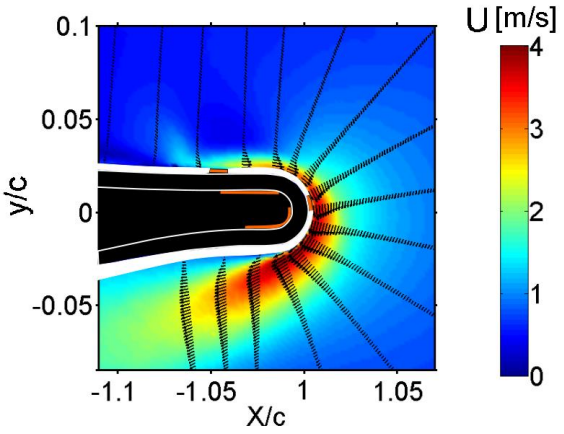

Figure 5. Time averaged magnitude velocity contours and velocity vector profiles of the flow induced by the DBD actuator (18 kV, 1 kHz).

The momentum coefficient C_μ, the typical figure of merit for discussing the circulation control efficiency, has been estimated. It was chosen to estimate the momentum coefficient by integration of the tangential velocity profile in the wall normal direction, in the plasma region, just at the downstream edge of the second grounded electrode, as done in [8] or [15].

$$C_\mu = \frac{\int_0^\infty \rho u^2(y)\, dy}{\frac{1}{2}\rho_\infty U_\infty^2 c} \quad (1)$$

Such actuators was previously characterised in a plane configuration [16] in terms of velocity profiles measured at different positions along the plasma region. Based on these results, for a freestream flow of U_∞ = 10 m/s, within this work, C_μ was about 0.004.

2.4. Continuous fluidic jet

Figure 6 shows the section view of the trailing edge airfoil median (z = 0 mm) section equipped with one of the fluidic jet orifices supplied with air from both ends of the airfoil. The airfoil is equipped with a spanwise distribution of 42 CJ located at *x*/c = 0.96 and spaced by λ = 21 mm. The squared hole area is S_{jet} = 1 mm².

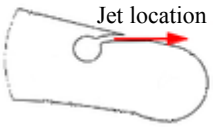

Figure 6. Fluidic jet orifice scheme close to the trailing edge.

The air system used to provide pressurized air to the actuators is composed of a compressor, a filtration system, a proportional valve and a volumetric flow meters (Q_v), which is used to evaluate the jet speed in computing the momentum coefficient derived from equation (2):

$$C_\mu = \frac{\rho_{jet}\, Q_v\, U_{jet}}{\frac{1}{2}\rho_\infty U_\infty^2 S} \quad (2)$$

where $S = \text{chord} \times \text{span}$. It is assumed that the jet is incompressible ($\rho_{jet} = \rho_\infty$). Using mass

conservation from the volumetric flow meter to the jet exit velocity of a transverse line, the jet speed can be estimated by equation (3):

$$U_{jet} = \frac{Q_v}{42 \times S_{jet}} \quad (3)$$

Within this study, it can be deduced that a value of $C_\mu = 0.0194$ for a freestream flow of U_∞ = 10 m/s, corresponding to a volumetric rate of 220 L/min.

The jet was characterized in quiescent air conditions using a laboratory-made total pressure (p_t) probe with an external diameter of 500 µm and an inner diameter of 250 µm ± 50 µm. It was placed on a 3D micro-displacement system with its axis in the longitudinal direction. The probe was connected to a Furness manometer through Tygon tubes. Considering its velocity, the flow at the exit of the controlled jet is assumed as incompressible, so that the reference static pressure is equal to the ambient pressure (p_o) and the jet exit speed is obtain using:

$$U_{jet} = \sqrt{\frac{2(p_t - p_0)}{\rho}} \quad (4)$$

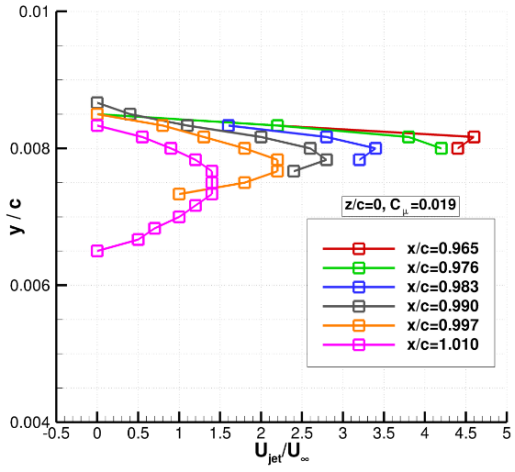

Figure 7. Longitudinal velocity profiles as a function of the vertical position y/c at different longitudinal positions x/c.

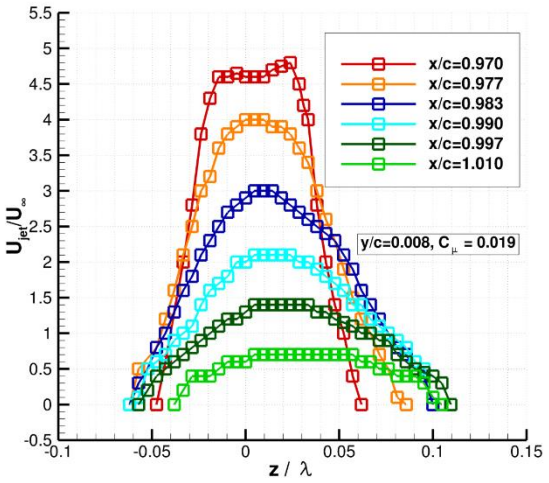

Figure 8. Longitudinal velocity profiles as a function of the transverse position z/c at different longitudinal positions x/c.

The mean spatial topology of a single jet was investigated in the vertical (y) (see figure 7) and in the spanwise (z) (see figure 8) direction at different longitudinal positions (x/c) in the median airfoil section, x/c = 1 corresponding to the position of the trailing edge end (see figure 2). The velocity value is non-dimensionalised by the freestream flow of 10m/s chosen for the circulation control results presented further. Firstly, results show that the jet is slightly deviated in the transverse and vertical directions. According to the vertical direction, the center of the jet is displaced by only 1.4 % of λ in the downward y direction (figure 7). According to the transverse direction, the center of the jet is displaced up to 3 % of λ towards positive values of z (figure 8). Then, it is clear that the jet speed rapidly decreases with the longitudinal direction. The velocity ratio $\frac{U_{jet}}{U_\infty}$ is equal to 4.5 at 2 jet diameters (or x/c = 0.965) and is equal to 2 at 14 jet diameters (or x/c = 1.005). Finally, by displacing the pressure probe in the spanwise direction at the maximum value of each jet exit velocity at x/d = 2 (with d the jet diameter), results exhibited a relatively low value of the standard deviation in the transverse direction of 13 %.

3. Results and discussions

3.1. Actuation effects on aerodynamic forces

For a Reynolds number of 2. 10^5, figure 9 shows the lift coefficient increment ΔC_L as a function of the angle of attack. A lift coefficient increase of 0.06 can be reached with both actuators even if the physical mechanisms of actuation are radically different (2D tangential jet for PA versus 3D jets for CJ). Whereas for PA, ΔC_L is constant with AOA, ΔC_L appears to slightly increase with AOA for CJ. It is likely that CJ reenergizes the boundary layer for higher AOAs and then contributes to delay its incipient separation.

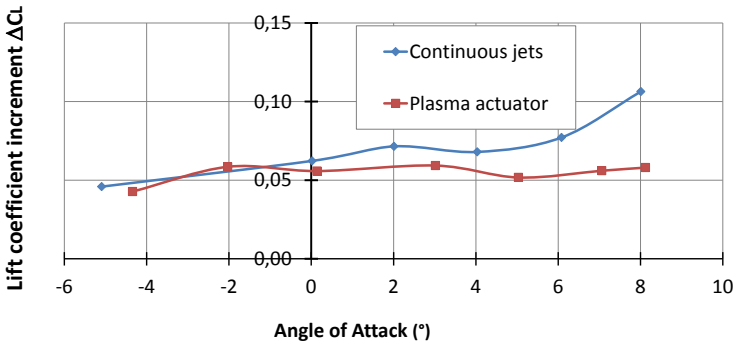

Figure 9. Increment of lift coefficient due to the actuation versus angle of attack for both actuations.

Static pressure measurements are used to highlight the modification of aerodynamic forces with actuation. Due to the PA implementation at the trailing edge, pressure measurements close to the trailing edge are not available and were consequently performed with pressure taps implemented around the model between the leading edge and x/c = 0.7. Mean pressure distribution for CJ is obtained from an averaged value of static pressure in the transverse direction (z). Close to the jet orifice, no pressure tap was available (around x/c = 0.9). In figure 10 the pressure distribution is plotted at U_∞ = 10 m/s without and with actuation. Slight differences can be observed on the wall static pressure distribution of the cases without actuation because of the different design and manufacture of both models and the selected AOA. Compared to the pressure distribution without actuation, the whole pressure distribution around the airfoil is modified. Pressure distribution is slightly decreased on the suction side and increased at the pressure side. With airfoil equipped with CJ, the same global trend is visible but it is completed by a local pressure suction peak at the trailing edge because the flow is accelerated by the momentum added by CJ. It is commonly observed in circulation control.

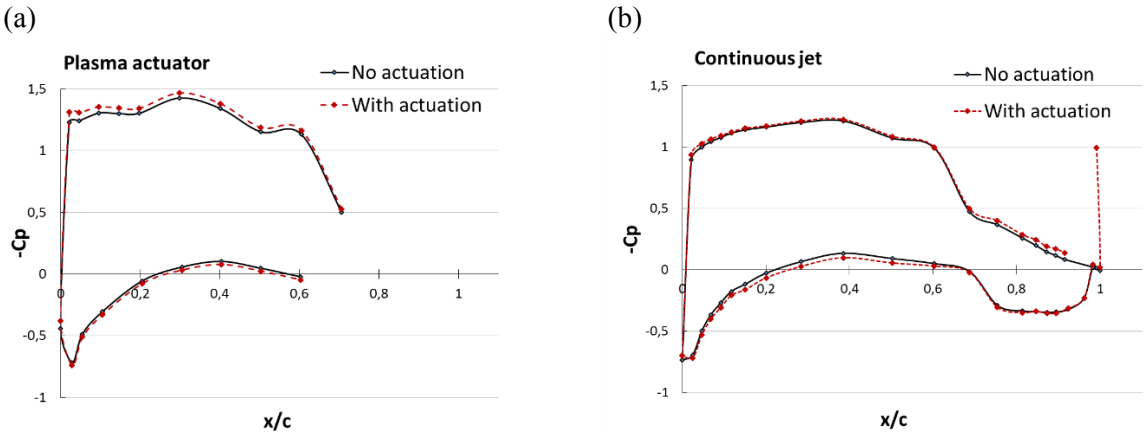

Figure10. Wall static pressure distributions at U_∞ = 10 m/s for (a) plasma actuation - AOA = 5 ° and (b) fluidic jet actuation - AOA = 4 °.

3.2. Actuation effects on the near wake

Figure 11 shows the flow around the airfoil trailing edge without actuation at an angle of attack of 5 ° and a Reynolds number equal to Re = 2. 10^5 by plotting mean time-averaged velocity contours and streamlines. It can be observed that the near wake, characterized by a recirculation zone due to the thick rounded trailing edge, develops on a length of 5 % of the chord. Streamlines enable to highlight the two counter-rotating structures similar to the ones that can be observed at the base of bluff bodies. Because of the 3D action on flow expected by CJ, the flow uniformity has been verified in the spanwise direction and is confirmed by the overlapping of the longitudinal u-velocity vertical profiles drawn in the near wake in figure 12 and derived from PIV measurements.

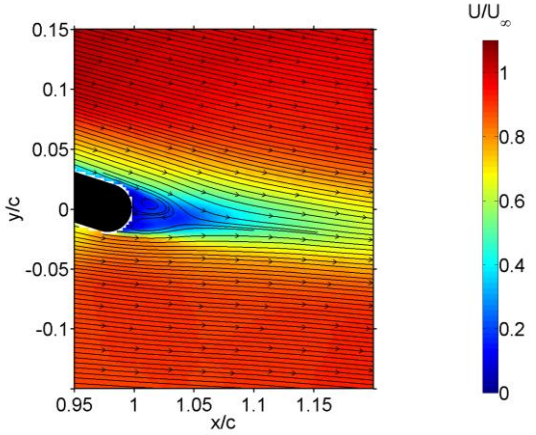

Figure 11. Topology of the baseline near wake in the centerline z = 0 mm. Time-averaged velocity contours and streamlines.

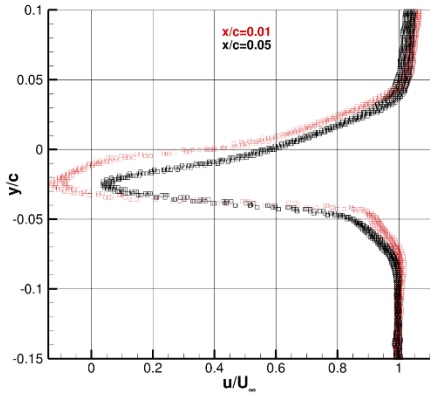

Figure 12. Overlapping of longitudinal u-velocity profiles versus vertical direction for transverse positions z = -9, -7, -4, 0, 3, 7, 9 mm, plotted for two longitudinal position x/c (CJ actuation).

Mean vertical v-velocity field contours and streamlines are plotted in figures 13, 14 and 15 to visualize the modification of the near wake topology due to both actuations. For PA and CJ, the vertical velocity is reinforced by the actuation downward the trailing edge meaning that the wake is deflected towards de pressure side of the airfoil. This leads to flow circulation modification around the airfoil. For PA (see figure 13), the two counter-rotating structures are not suppressed whereas for CJ, depending on the transverse position z, they disappear (see figure 15 (b)) and the flow is quite fully reattached along the round trailing edge at z = 7 mm.

Figure 16 zooms in on longitudinal u-velocity profiles in the near wake at the streamwise location x/c = 1.05 in the recirculation area. It can be observed a change of the recirculation area due to the actuation. For PA more particularly, the maximum longitudinal velocity deficit slightly moves downward, establishing the wake deflection due to the plasma actuation. For CJ, due to the 3D action, it can be observed strong shear region in which streamwise vortices develop. The signature of the continuous jet shows up around y/c = 0 and the ones of the wake around y/c = -0.025. As previously seen in the velocity field in figures 14 and 15, the flow can be reattached between two jets according to the transverse position. Consequently the velocity deficit is more or less important in figure 16 (b).

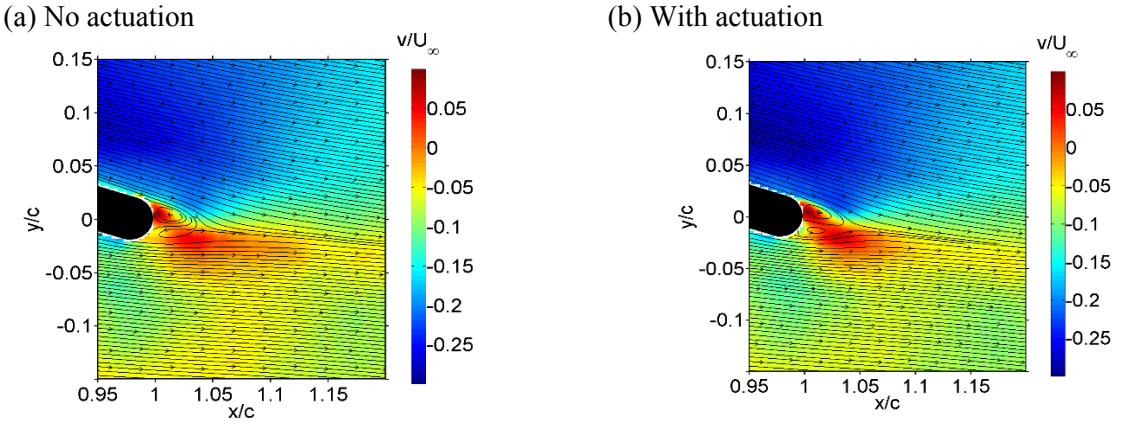

Figure 13. Vertical v-velocity field contours and streamline for the transverse section z = 0 mm **(**a) without and (b) with actuation for plasma actuation, Re = 2. 10^5, AOA = 5 °.

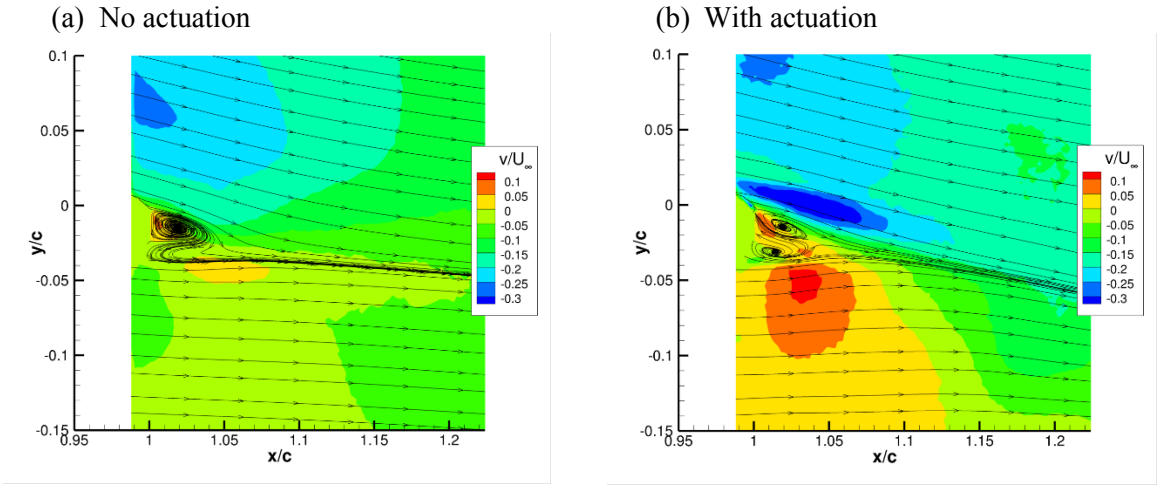

Figure 14. Vertical v-velocity field contours and streamlines for the transverse section z = 0 mm (a) without and (b) with actuation for continuous jets, Re = 2. 10^5, AOA = 5 °.

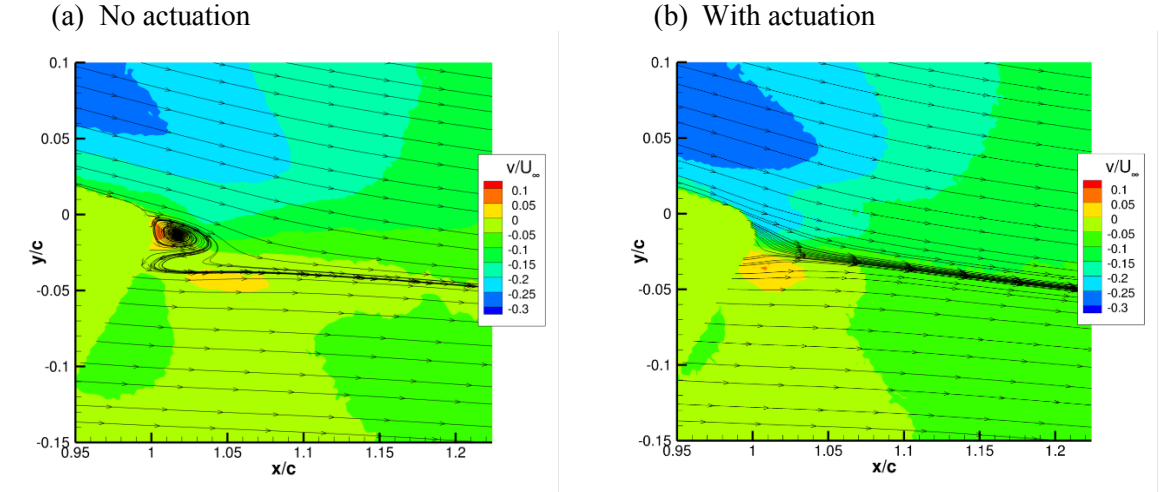

Figure 15. Vertical v-velocity field contours and streamlines for the transverse section z = 7 mm (a) without and (b) with actuation for continuous jets, Re = 2. 10^5, AOA = 5 °.

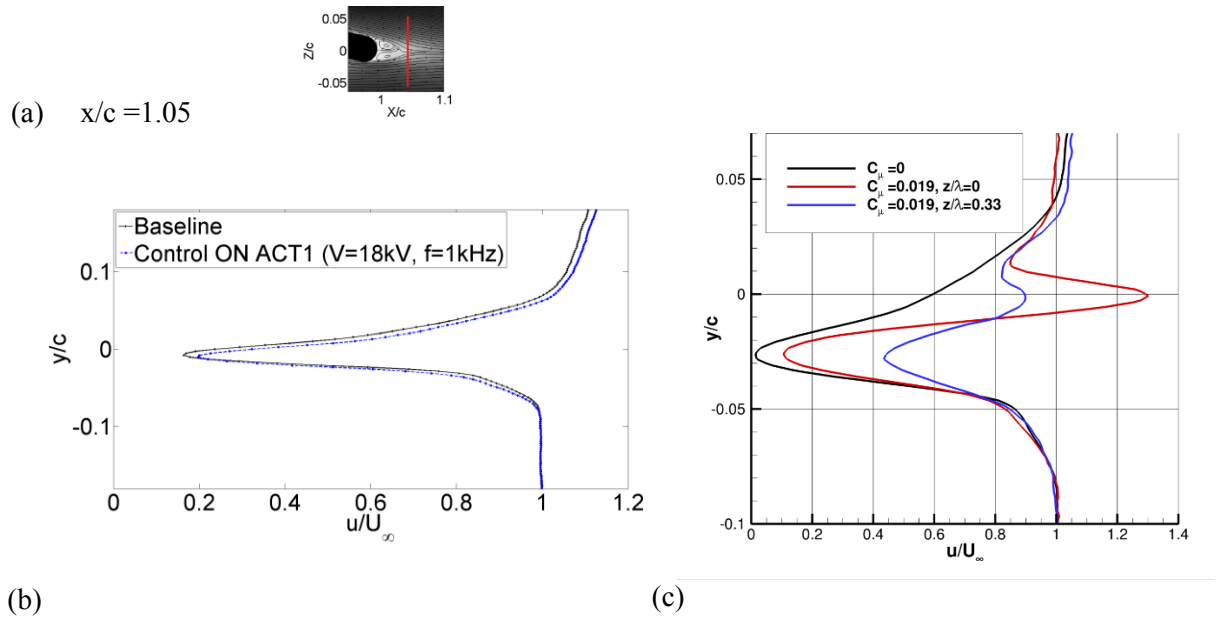

Figure 16. Time averaged longitudinal u-velocity component versus y/c at (a) x/c =1.05 for (b) plasma actuation and (c) fluidic jet, Re = 2. 10^5, AOA = 5 °.

4. Conclusion

This study has provided first results in analysing lift increase achieved by two methods of active flow control acting at a rounded trailing edge of a wind turbine blade airfoil. Two types of actuators are used in this circulation control application, DBD actuator and continuous jet distribution. They allow lift increase monitoring by involving different mechanisms of interaction with the natural flow. DBD actuator are supposed to act as a bi-dimensional wall jet and continuous jets have a three-dimensional action on the flow probably characterised by the presence of generate streamwise vortices. In order to refine the understanding of the mechanisms, further analysis and investigation are in progress to highlight streamwise vortices between holes by PIV measurements in transverse plans, as well as temporal measurements to observe the vortex shedding alteration under actuation effects.

In the objective of reducing the load fluctuations on the blades, it is expected that the control technique can also decrease the lift. This work is in current investigation by implementing actuators so that they produce a wall jet in the reverse direction as described in [17] for plasma actuators. Finally, control efficiency of these methods of active flow control will be discussed in view of load alleviation for wind turbines blades.

Acknowledgements

This project is funded by the national French project SMARTEOLE (ANR-14-CE05-0034).

References

[1] Joslin R D and Jones G S 2006 *Progress in astronautics and aeronautics* **214** AIAA Inc
[2] Kweder J, Panther C C and Smith J E 2010 *Int. J. Eng* **4** 411–429.
[3] Dumitrache A, Frunzulica F, Dumitrescu H, Cardos V 2014 *Incas Bulletin* **6** 2 33 – 49 ISSN 2066 – 8201.
[4] Johnson S J, Case van Dam CP and D.E. Berg D E 2008 Active Load Control Techniques for Wind Turbines *SANDIA Report*
[5] Corke T C, Enloe C L and Wilkinson S P 2010 *Ann. Rev. of Fluid Mech.* **42** 1 505–529

[6] Bénard N and Moreau E 2014 *Exp. in Fluids* 55:1846
[7] Wang J J, Choi K S, Feng L H, Jukes T N and Whallley R D 2013 *Prog. in Aerospace Sciences* **62** 52-78
[8] Zhang P F., Yan B, Liu A B and J. J. Wang J J 2010 *AIAA Journal* **48** 10
[9] Kotsonis M, Pul R and Veldhuis L 2014 *Exp. in Fluids* **55**:1772
[10] Compton D and Johnston J 1992 *AIAA Journal* **30**
[11] Cathalifaud P, Godard G, Braud C and Stanislas M 2009 *J. of Turbulence* **10** 42
[12] Laval J, Braud C, Fournier G and Stanislas M 2010 *J. of Turbulence* **11**
[13] Cuvier C, Braud C, Foucault J and Stanislas M 2011 *7th Turb. And Shear Flow Phenomena* Ottawa-Canada
[14] Taylor Z J, Gurka R Kopp G A and Liberzon A 2010 *IEEE Trans. on Instrumentation and Measurement* **59** 12 3262-3269
[15] Roberto Sosa R, Artana G, Moreau E and Touchard G 2007 *Exp. in Fluids* **42** 143–167
[16] Leroy A, Podlinski J, Baleriola S, Devinant P and Aubrun S 2016 *International Journal of Plasma Environmental Science & Technology* to be published
[17] Baleriola S, Leroy A, Loyer S, Devinant P and Aubrun S 2016 *Proc. In TORQUE 2016*